Materials Chemistry and Physics 111 (2008) 143–148

Contents lists available at ScienceDirect

Materials Chemistry and Physics

journal homepage: www.elsevier.com/locate/matchemphys

Studies on red-emitting Cr^{3+} doped barium aluminate phosphor obtained by combustion process

Vijay Singh [a], R.P.S. Chakradhar [b], J.L. Rao [c], Jun-Jie Zhu [a,*]

[a] Key Lab of Analytical Chemistry for Life Science, School of Chemistry and Chemical Engineering, Nanjing University, Nanjing 210093, PR China
[b] Glass Technology Lab, Central Glass and Ceramic Research Institute, Kolkata 700032, India
[c] Department of Physics, Sri Venkateswara University, Tirupati 517502, India

ARTICLE INFO

Article history:
Received 12 December 2007
Received in revised form 11 March 2008
Accepted 27 March 2008

Keywords:
Phosphors
EPR
Photoluminescence
Combustion
Cr^{3+} ions

ABSTRACT

Red-emitting $BaAl_2O_4:Cr^{3+}$ phosphor material is prepared by urea combustion route in 5 min. Powder X-ray (XRD) diffraction, thermogravimetric analysis (TGA), scanning electron microscopy (SEM) and BET surface area measurements are used to characterize the as-prepared combustion products. Electron Paramagnetic Resonance (EPR) studies have been carried out on Cr^{3+} ions in $BaAl_2O_4$ phosphors at room temperature and at 110 K. The number of spins participating in resonance (N) and its paramagnetic susceptibilities (χ) have also been evaluated. The excitation spectra shows two broad and intense bands corresponding to Cr^{3+} ion in octahedral symmetry. The red emission peak observed at 705 nm is identified as due to $^2E_g \rightarrow {}^4A_{2g}$ transition from Cr^{3+} ions. The crystal field parameter Dq and Racah inter-electronic repulsion parameters B and C have been evaluated. From the results and analyses of the EPR and optical studies, the site symmetry of Cr^{3+} ion in this phosphor is attributed to a distorted octahedron.

1. Introduction

Trivalent chromium (Cr^{3+}) is the most stable oxidation state of chromium, therefore widely used as a luminescent dopant and luminescence sensitizer in various materials. Chromium is a low cost activator, which can provide deep color and bright luminescence. For instance, the color of many natural and synthetic gemstones like ruby, emerald, alexandrite, etc., is caused by Cr^{3+} ions. On this account, Cr^{3+} is subject of numerous optical spectroscopic and luminescence investigations. Further, Cr^{3+} doped systems are used in modern technologies, for example, tunable solid-state lasers [1], high temperature sensors [2,3], and high-pressure calibrants [4]. Recently, significant efforts have been devoted by several research groups on the synthesis and characterization of various Cr^{3+} doped host materials. They have investigated Cr^{3+} emission in several compounds like $BeAl_2O_4$ [5], $ZnAl_2S_4$ [6], $Y_3Al_5O_{12}$ [7], $MgAl_2O_4$ [8], Al_2O_3 [9], $CaYGdAlO_4$ [10], $LiAlO_2$ [11], $ZnGa_2O_4$ [12], $LiTaO_3$ [13], $LiNbO_3$ [14], $LaSc_3(BO_3)_4$ [15], Mg_2SiO_4 [7], Cs_2NaYBr_6 [16], Cs_2NaYCl_6 [16], $Cs_2NaScCl_6$ [17], Cs_2NaGaF_6 [18], $KMgF_3$ [19], etc. There are few reports available on Cr^{3+} emission in aluminates using low temperature synthesis method [20–22].

Recent investigations have focused extensively on various aluminates as hosts for luminescent materials doped with transition metal or rare earth ions. It was noted that these aluminates have been prepared traditionally by solid-state reactions [23–25], which demand, generally, long times and high annealing temperatures, 5–10 h and 1300–1700 °C. Further in some of the preparation methods, in order to obtain final product, repeated heating, special equipment and expensive raw materials were needed. Indeed there is growing demand for economically viable synthesis methods for producing the various aluminates. Combustion synthesis is very useful from this point of view. In this work, we have successfully employed relatively a low temperature, fast, simple and safe combustion process for the preparation of Cr^{3+} doped $BaAl_2O_4$ material. The prepared samples were characterized by X-ray diffraction (XRD), Thermogravimetric analysis (TGA), Scanning electron microscopy (SEM), BET surface area measurements, UV–vis absorption spectroscopy, Photoluminescence (PL) and Electron paramagnetic resonance (EPR) techniques.

2. Experimental

Cr^{3+} doped aluminates were prepared using combustion synthesis, which involves heating of metal nitrate and aluminium nitrate in stochiometric proportions with fuels such as urea at temperature around 500 °C. In the present investigation, materials were prepared according to the chemical formula $Ba_{1-x}Cr_xAl_2O_4$ where $x = 0.01$ mol%. More details about combustion synthesis can be found in the original paper [26]. The compounds, so prepared, were identified using XRD technique. Pow-

* Corresponding author. Tel.: +86 25 83594976; fax: +86 25 83594976.
E-mail address: jjzhu@mail.nju.edu.cn (J.-J. Zhu).

0254-0584/$ – see front matter © 2008 Elsevier B.V. All rights reserved.
doi:10.1016/j.matchemphys.2008.03.033

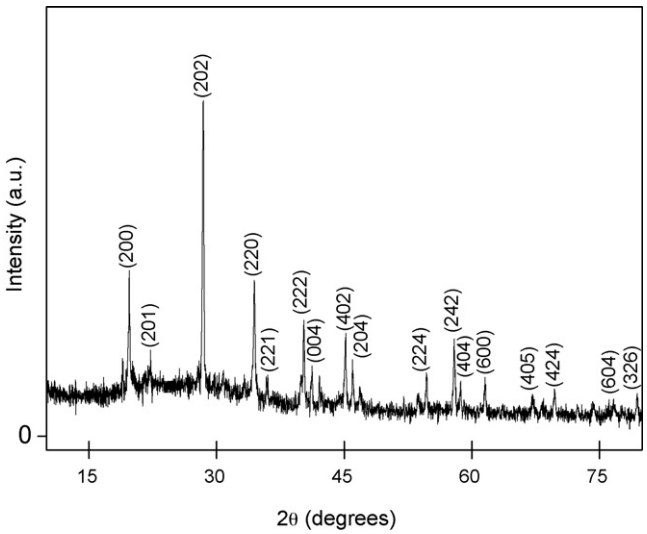

Fig. 1. XRD patterns of $Ba_{0.99}Cr_{0.01}Al_2O_4$.

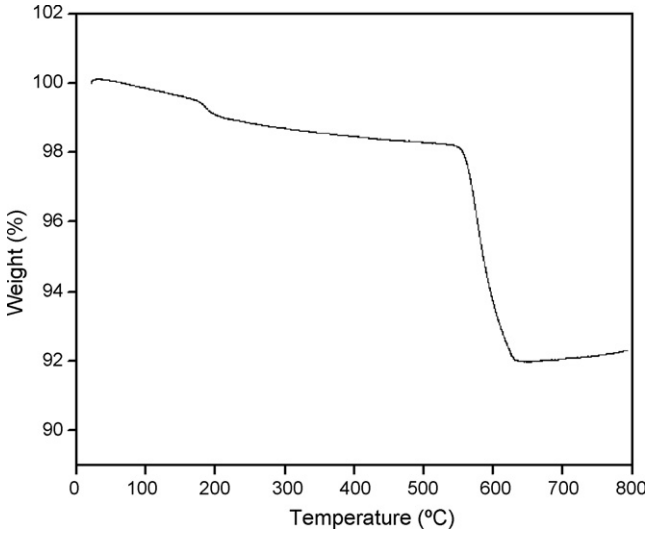

Fig. 2. Thermogravimetric curve of the combustion prepared $Ba_{0.99}Cr_{0.01}Al_2O_4$ (heating rate 10 °C min^{-1}; gas flow-rate: 40 ml min^{-1}; N_2).

der XRD pattern was recorded on a Philips X′ pert X-ray diffractometer with graphite monochromatized Cu Kα radiation (λ = 0.15418 nm) and nickel filter at a scanning step of 0.03°, continue time 10 s, in the 2θ range from 10° to 80°. Thermo-analysis was carried out with a PerkinElmer themoanalyzer. The combustion reaction was studied between 20 and 800 °C, with a heating rate 10 °C min^{-1} and the gas (N_2) flow-rate was 40 ml min^{-1}. Scanning electron micrographs (SEM) were taken on a JEOL JSM-5610LV scanning electron microcopy. The BET surface area measurements were done by nitrogen adsorption employing a Micromeritics Accusorb ASAP 2020 instrument. Shimadzu UV-2401 spectrophotometer was used to record the UV–vis absorption spectra. PL measurements were carried out on an AMINCO-Bowman Series 2 luminescence spectrometer at room temperature and also performed with a confocal laser micro-Raman spectrometer (Raman, LABRAM-HR) with 488 nm laser excitation. EPR measurements were carried out on a Bruker EMX 10/12 X-band ESR spectrometer.

3. Results and discussion

3.1. XRD analysis

The XRD pattern of as-prepared $BaAl_2O_4:Cr^{3+}$ powder phosphor is shown in Fig. 1. All the major reflections in Fig. 1 could be indexed to the standard hexagonal $BaAl_2O_4$ (JCPDS, 71-1323). The lattice parameters calculated for hexagonal $BaAl_2O_4$ were $a = b = 10.41$ Å and $c = 8.76$ Å. The prepared materials are fully crystalline at furnace temperature 500 °C and therefore, the post-crystallization heat-treatments are not required. The peak at 28.43° was the most intensive and the crystal size was calculated through it using the Scherrer's formula. The crystal size of the $BaAl_2O_4$:Cr was calculated to be 46 nm.

3.2. TGA measurement

The thermogravimetric curve (Fig. 2) of as-prepared Cr^{3+} doped $BaAl_2O_4$ phosphor shows two step weight loss observed in the temperature between 20 and 665 °C. The TG pattern shows minor (0.92%) weight loss in the temperature range 130–250 °C, which may be attributed to the removal of moisture. Further, weight loss (6.26%) corresponding to the decomposition of metal nitrate is observed in the temperature range 520–665 °C. It is noted that in our system there is no evidence for compound formation in TG experimental results. This clearly shows that the compound formation occurs at high temperature.

3.3. SEM and BET measurements

Fig. 3 shows the SEM micrographs of the $BaAl_2O_4:Cr^{3+}$ phosphor with low- and high-magnification. Reaction in the presence of urea allows the growth of faceted crystals. It exhibited most of the aluminates took the form of platelets with rough surfaces. It is noticed that with high-magnification, single platelet shows a number of voids and pores, which result from the escaping gases during combustion. The BET surface area of as-prepared Cr^{3+} doped $BaAl_2O_4$ phosphor is 7.68 m^2 g^{-1}. Earlier, Kingsley et al. [20] reported the specific surface area of pure $BaAl_2O_4$ phosphor, prepared by the urea process, as 2.01 m^2 g^{-1}. The cause of enhancement in surface area value in our sample may probably be associated with Cr doping. However, in order to resolve the issue of enhancement in surface area there is need of more studies.

3.4. Electron paramagnetic resonance study

Fig. 4 shows the EPR spectrum of $BaAl_2O_4:Cr^{3+}$ phosphors at (a) room temperature and (b) at 110 K. Chromium ion belongs to $3d^3$ electronic configuration and according to Hund's rule the ground state is ^4F. In an octahedral crystal field, this state splits into an orbital singlet $^4A_{2g}$ and two orbital triplets $^4T_{1g}$ and $^4T_{2g}$ [27]. In a distorted octahedral site, the electronic levels can be described by a spin–Hamiltonian of the form [28,29]

$$H = ßBgS + D\left[S_z^2 - \left\{\frac{S(S+1)}{3}\right\}\right] \quad (1)$$

where the first term represents the electronic Zeeman term, second term characterizes the zero-field splitting of the quartet ground state. In the absence of an external magnetic field B; the four fold spin degeneracy of the $^4A_{2g}$ state is removed by a subsequent low symmetric field resulting in a zero-field splitting of the Kramers doublets $|\pm 3/2>$ and $|\pm 1/2>$. In the presence of a magnetic field, the degenerate doublets split further. On applying a microwave frequency field, a transition with $\Delta m_s = \pm 1$ may be observed in the EPR spectra. However, the number of resonance signals depend upon the magnitude of the zero-field splitting for a given photon energy [30].

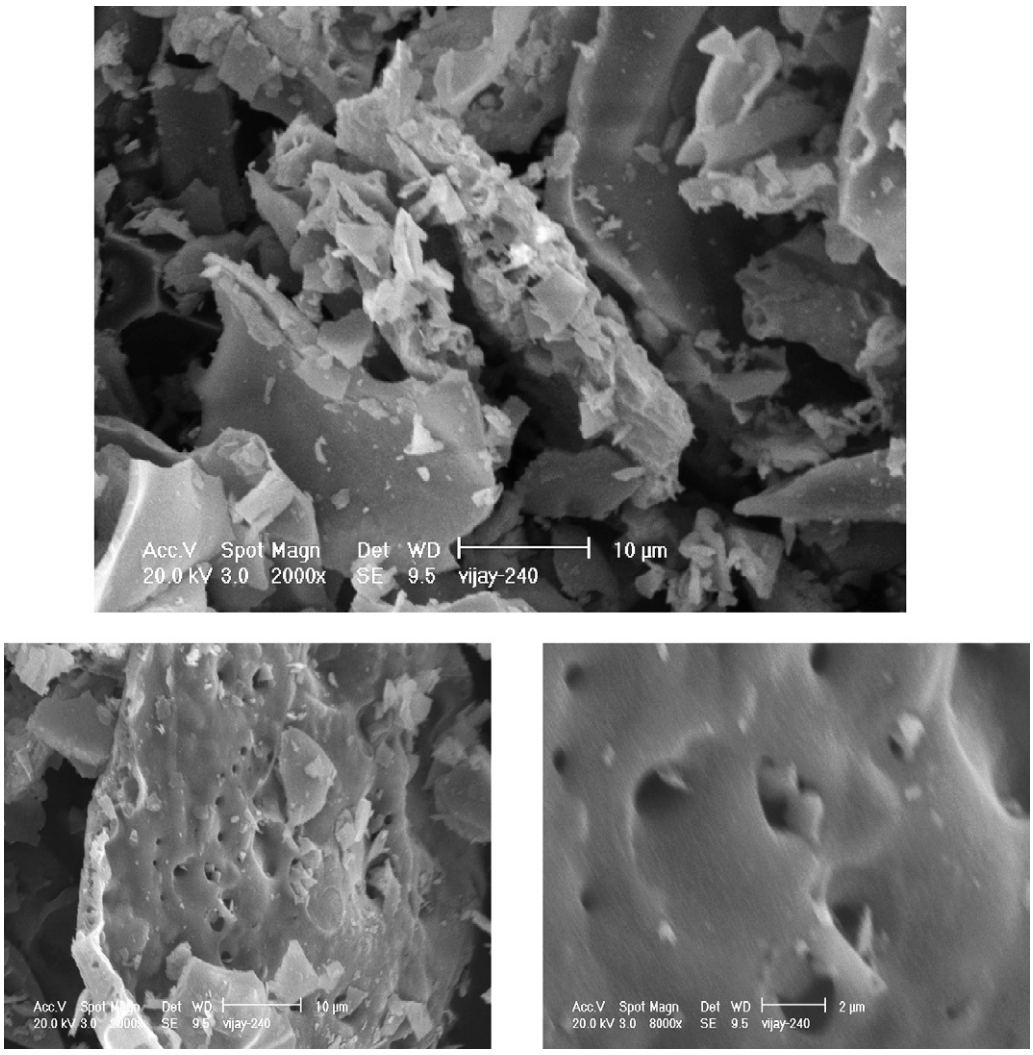

Fig. 3. SEM micrographs of the $Ba_{0.99}Cr_{0.01}Al_2O_4$, at low- and high-magnification.

In the present study, the EPR spectra of the investigated $BaAl_2O_4$:Cr phosphor exhibit resonance signals as shown in Fig. 4. The EPR spectra of the investigated phosphor exhibit a broad resonance signal at $g = 4.93$ and an intense resonance line centered at $g = 1.95$. The spectrum at low field side, i.e., the EPR absorption at the resonance signal at $g = 4.93$ is attributed to isolated Cr^{3+} ions whereas the resonance signal at $g = 1.95$ is attributed to exchange coupled Cr^{3+} ion pairs and is related to strongly distorted sites. A resonance signal (at $g = 2.26$) on the immediate lower magnetic field side of $g = 1.95$ is observed. This resonance signal arises due to large separation between the two Kramers doublets [27]. The EPR signals appear in the range of low magnetic fields with a resonant field of 130–170 mT indicates that the zero-field splitting, 2D of the $^4A_{2g}$ single orbital state is relatively large in comparison with the energy of the microwave radiation used in the X-band ESR spectrometer.

3.4.1. Calculation of number of spins (N) participating in resonance

The number of spins participating in resonance can be calculated by comparing the area under the absorption curve with that of a standard ($CuSO_4{\cdot}5H_2O$ in this study) of known concentration. Weil et al. [31] gave the following expression which includes the experimental parameters of both sample and standard.

$$N = \frac{A_x(\mathrm{Scan}_x)^2 G_{\mathrm{std}}(B_{\mathrm{m}})_{\mathrm{std}}(g_{\mathrm{std}})^2[S(S+1)]_{\mathrm{std}}(P_{\mathrm{std}})^{1/2}}{A_{\mathrm{std}}(\mathrm{Scan}_{\mathrm{std}})^2 G_x(B_{\mathrm{m}})_x(g_x)^2[S(S+1)]_x(P_x)^{1/2}}[\mathrm{Std}] \qquad (2)$$

where A is the area under the absorption curve, which can be obtained by double integrating the first derivative EPR absorption curve, scan is the magnetic field corresponding to a unit length of the chart, G is the gain, B_{m} is the modulation field width, g is the g factor, S is the spin of the system in its ground state. P is the power of the microwave source. The subscripts 'x' and 'std' represent the corresponding quantities for the $BaAl_2O_4$:Cr phosphor and the reference ($CuSO_4{\cdot}5H_2O$), respectively. The value of N has been calculated for $g = 1.95$ for the studied phosphor at room temperature and also at 110 K and are presented in Table 1. It is observed

Table 1
The number of spins (N) participating in resonance and paramagnetic susceptibility (χ) for the resonance signal at $g = 1.95$ for $Ba_{0.99}Cr_{0.01}Al_2O_4$ phosphor at room temperature and at 110 K

System	Temperature (K)	$g = 1.95$	
		$N \times 10^{21}$ (arb. units)	$\chi \times 10^{-4}$ m^3 Kg^{-1}
$Ba_{0.99}Cr_{0.01}Al_2O_4$	300	1.42	3.29
$Ba_{0.99}Cr_{0.01}Al_2O_4$	110	2.49	5.77

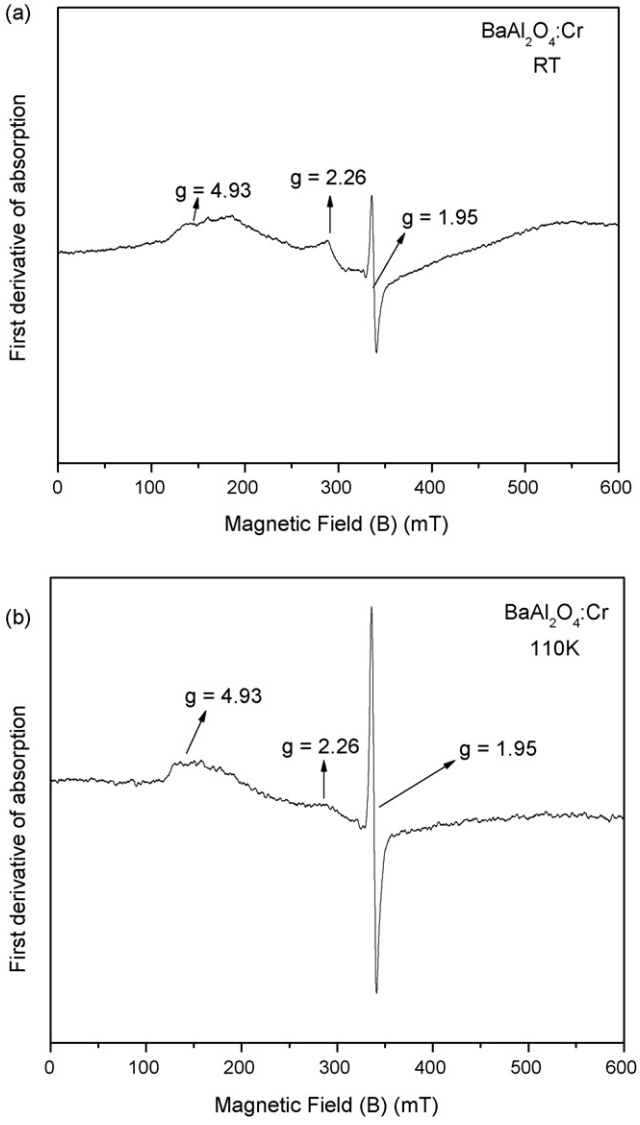

Fig. 4. EPR spectrum of $Ba_{0.99}Cr_{0.01}Al_2O_4$ at (a) Room temperature and (b) 110 K.

that as the temperature is lowered, N increases obeying the Boltzmann law.

3.4.2. Calculation of paramagnetic susceptibility (χ) from EPR data

The EPR data can be used to calculate the paramagnetic susceptibility of the sample using the formula [32]

$$\chi = \frac{Ng^2\beta^2 J(J+1)}{3k_B T} \quad (3)$$

where N is the number of spins per m^3 and the other symbols have their usual meaning. N can be calculated from Eq. (2) and g is taken from EPR data. Since the intensity of the resonance signal at $g = 1.95$ is greater when compared to the resonance signal at $g = 4.93$, the value of $g = 1.95$ is used in calculating the paramagnetic susceptibility values. The paramagnetic susceptibility (χ) values evaluated from EPR data are also presented in Table 1.

The crystal structure of $BaAl_2O_4$ (spinel) belongs to $A^{2+}B^{3+}O_4$ and the spinel unit cell belongs to the cubic space group O_h^7 (Fd3 m) with eight formula units per cell. The A site (Ba or Mg) has tetrahedral coordination with full T_d site symmetry, while the B site (Al or Ga) has six fold distorted octahedral coordination belongs to the

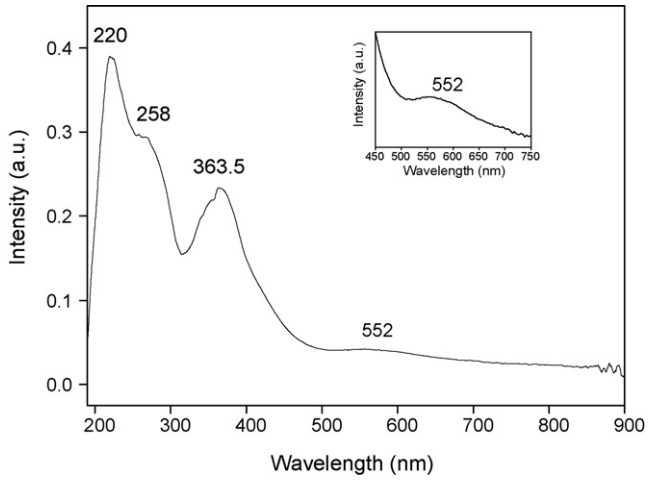

Fig. 5. The UV–vis absorption spectrum of $Ba_{0.99}Al_2O_4$:$Cr_{0.01}$.

D_{3d} point group [33–35]. In the case of the Cr^{3+} ion in spinels, the Cr^{3+} ion which has high octahedral site preference energy [35], are preferred to occupy octahedral B sites in spinels and form normal spinels.

3.5. Optical properties

3.5.1. UV–vis absorption study

The room temperature absorption spectrum of $BaAl_2O_4$:Cr^{3+} is shown in Fig. 5. The absorption spectrum consists of peaks at 220 nm (45,440 cm^{-1}), 258 nm (38,748 cm^{-1}), 363.5 nm (27,540 cm^{-1}) and 552 nm (18,110 cm^{-1}). The broad absorption band observed at 552 nm has been attributed to Cr^{3+} ions in octahedral symmetry. Cr^{3+} ions belong to d^3 configuration, the ground state is always $^4A_{2g}(F)$ irrespective of strength of crystal field. In general Cr^{3+} ions are characterized by three spin allowed transitions $^4A_{2g}(F) \rightarrow {}^4T_{2g}(F)$, $^4A_{2g}(F) \rightarrow {}^4T_{1g}(F)$ and $^4A_{2g}(F) \rightarrow {}^4T_{1g}(P)$. In addition to this, a number of doublet states also possible, which are spin-forbidden transitions. In the present study, a broad band is observed at 552 nm. The intensity and position of this main band suggest that this band to be related to d–d electronic transition and is assigned to the transition $^4A_{2g}(F) \rightarrow {}^4T_{2g}(F)$ of Cr^{3+} ions in octahedral symmetry. The other bands at 363.5, 258 and 220 nm have been assigned to charge transfer bands of CrO^{6+}–O^{2-} and Al–O.

3.5.2. Photoluminescence study

The excitation and emission spectra for $BaAl_2O_4$:Cr^{3+} phosphor are shown in Figs. 6(a) and (b), respectively. The excitation spectrum exhibits two broad intense bands located at 421 nm (23,750 cm^{-1}) and 552 nm (18,110 cm^{-1}). These bands have been assigned to the transitions $^4A_{2g}(F) \rightarrow {}^4T_{1g}(F)$ and $^4A_{2g}(F) \rightarrow {}^4T_{2g}(F)$, respectively. The observed peaks coincide with the excitation peaks reported by Yamaga et al. [36]. Berger [33] and Wood et al. [34] also observed similar transitions in Cr^{3+} doped $MgAl_2O_4$ spinels. In addition to two intense bands, two small humps at 494 nm (20,240 cm^{-1}), 483 nm (20,700 cm^{-1}) and a sharp band at 467 nm (21,410 cm^{-1}) have been observed in the excitation spectrum of $BaAl_2O_4$:Cr^{3+} phosphor. These bands are denoted as B1, B2 and B3, respectively (Fig. 6(a)). The intensity and position of this sharp band at 467 nm is assigned to the spin forbidden transition $^4A_{2g}(F) \rightarrow {}^2T_{2g}(F)$. The two small humps cannot be assigned to d–d electronic transition and they may be due to some unknown impurity in the sample. Fig. 6(b) and (c) show the emission spectrum with a doublet at 701 nm (14,261 cm^{-1}) and 705 nm (14,180 cm^{-1}). Such a doublet, i.e., an intense R1 line (705 nm) and

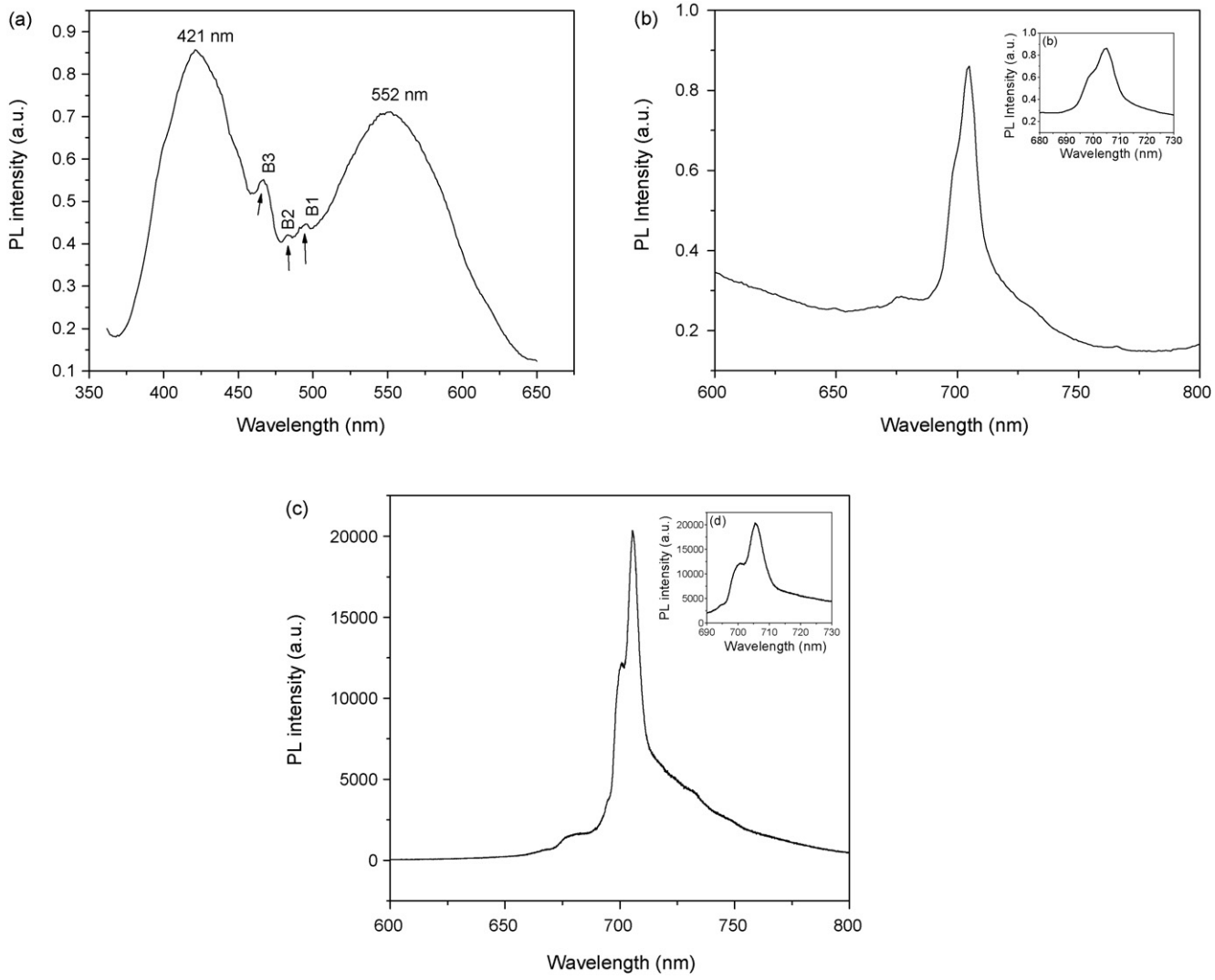

Fig. 6. Typical photoluminescence spectra of Cr^{3+} doped $BaAl_2O_4$: (a) excitation spectrum of $Ba_{0.99}Al_2O_4:Cr_{0.01}$ (λ_{em} = 705 nm), (b) emission spectrum of $Ba_{0.99}Al_2O_4:Cr_{0.01}$ (λ_{ex} = 421 nm) and (c) emission spectrum of $Ba_{0.99}Al_2O_4:Cr_{0.01}$ (Laser λ_{ex} = 488 nm) (inset shows the enlarged portion of $^2E_g \rightarrow {}^4A_{2g}$ transition from Cr^{3+} ions).

partly frozen out R2 line (701 nm) is characteristic of Cr^{3+} ions which is caused by the spin-forbidden $^2E_g \rightarrow {}^4A_{2g}$ transition. Some of the weaker and broader side bands are obviously phonon satellites of these later zero-phonon transitions R1 and R2. Kingsley et al. [20] observed a red emission at 687 nm in $MgAl_2O_4$ lattice which has been attributed as due to the Cr^{3+} substituted in O_h sites of Al^{3+} ions [20]. Broad absorption bands, which give the red color in aluminates, have been reported by Ford and Hill [35] for $MgAl_2O_4:Cr^{3+}$.

The authors also performed photoluminescence studies, on $BaAl_2O_4:Cr^{3+}$ phosphors using a confocal laser micro-Raman spectrometer (Raman, LABRAM-HR) with 488 nm laser excitation. It also confirms the red emission in these $BaAl_2O_4:Cr^{3+}$ phosphors at 705 nm due to $^2E_g \rightarrow {}^4A_{2g}$ transition with R lines. The excitation spectral data were used to calculate the crystal field parameters using Tanabe–Sugano matrices [37]. Dq and B were determined from the $^4T_{2g}$ (F) and $^4T_{1g}$(F) band position, respectively. C was varied to provide the best fit to the $^2T_{2g}$ transition energy. The resulting energies and the crystal field parameters are presented in Table 2. The observed band positions and energy level splittings are in good agreement with the value reported in literature [38]. The parameter B is found to be $B = 533\ cm^{-1}$. The value of inter-electronic repulsion parameter B for the Cr^{3+} free ion is 918 cm^{-1} [39]. A comparison with the observed B value (533 cm^{-1}) indicates that the B value is decreased by 42%. This might be due to bonding effects.

In the Tanabe–Sugano diagram, the crossing of the ^2E_g and $^4T_{2g}$ levels occurs near $Dq/B = 2.3$. The values higher than 2.3 correspond to strong ligand field sites [40]. If Cr^{3+} ions are in the strong ligand field sites, ^2E_g is the lowest excited state. In the present work no bands were observed on the lower energy side of the $^4T_{2g}$ band. This confirms that the two small humps denoted as B_2 and B_3 in Fig. 6(a) cannot be assigned to d–d electronic transitions ($^2T_{1g}$ and ^2E_g states) and these two small humps may be due to impurities present in the samples. The ratio Dq/B in the present work is found

Table 2
Observed and calculated energy values, crystalfield (Dq) and Racah parameters (B and C) from the excitation spectrum of the $BaAl_2O_4:Cr^{3+}$ phosphors

Transition from $^4A_{2g}$(F)	Observed (cm^{-1})	Calculated (cm^{-1})
$^4T_{2g}$(F)	18,110	18,110
$^2T_{2g}$(G)	21,410	21,490
$^4T_{1g}$(F)	23,750	23,750

($B = 533\ cm^{-1}$, $C = 2862\ cm^{-1}$, $Dq = 1811\ cm^{-1}$ and $Dq/B = 3.4$).

to be 3.42. The position of the bands together with the ratio Dq/*B* being higher than 2.3 indicates that the Cr^{3+} ions are in the strong ligand field sites.

4. Conclusions

It is possible to obtain Cr^{3+} ions doped $BaAl_2O_4$ red-emitting phosphors using a combustion synthesis method involving temperatures about 500 °C in a short time (<5 min). The advantages of the combustion synthesized include procedural simplicity and economy of the method as the starting materials are cheap and easy available. The XRD data show hexagonal phase for $BaAl_2O_4$. SEM micrographs indicate that, aluminates took the form of platelets with rough surfaces and single platelet shows a number of voids and pores. It is observed that the surface area increased with Cr doping. The EPR spectra exhibit a broad resonance signal at $g = 4.93$ and a sharp signal at $g = 1.95$. The resonance at $g = 4.93$ is attributed to isolated Cr^{3+} ions in rhombic symmetry subjected to strong crystal field effects and the $g = 1.97$ is due to exchange coupled Cr^{3+} ion pairs. The red emission peak, observed at 705 nm in $BaAl_2O_4$:Cr^{3+}, was identified as due to $^2E_g \rightarrow {}^4A_{2g}$ transition from Cr^{3+} ions. From the excitation spectrum the crystal field splitting (Dq) and Racah inter-electronic repulsion parameters (*B* and *C*) have been evaluated. The ratio Dq/*B* indicates that Cr^{3+} ions are in strong ligand field sites.

Acknowledgments

This work was supported by the National Natural Science Foundation of China (Grant Nos. 20635020, 20575026 and 90606016) and Jiangsu Natural Science Foundation of China (BK2006114). Dr. RPSC thanks Dr. H. S. Maiti, Director CGCRI and Dr. Ranjan Sen, Head, Glass Technology Laboratory, CGCRI for their constant encouragement.

References

[1] B. Struve, G. Huber, J. Appl. Phys. 57 (1985) 45.
[2] Z.Y. Zhang, K.T.V. Grattan, A.W. Palmer, V. Fernicola, L. Crovini, Phys. Rev. B 51 (1995) 2656.
[3] K.T.V. Grattan, R.K. Selli, A.W. Palmer, Rev. Sci. Instrum. 59 (1988) 1328.
[4] P.R. Wamsley, K.L. Bray, J. Lumin. 59 (1994) 11.
[5] O.A. Plaksin, V.A. Stepanov, P.A. Stepanov, V.M. Chernov, V.A. Skuratov, J. Nucl. Mater. 233 (1996) 1355.
[6] E. Broussell, L. Fortina, S. Kulyuk, A. Popov, R. Anedda, Corpino, J. Appl. Phys. 84 (1998) 531.
[7] S.M. Kaczmarek, W. Chen, G. Boulon, Cryst. Res. Technol. 41 (2006) 41.
[8] The-Long Phan, Manh-Huong Phan, Seong-Cho Yu, Phys. Stat. Sol. (b) 241 (2004) 434.
[9] R. Krishnan, R. Kesavamoorthy, S. Dash, A.K. Tyagi, Baldev Raj, Scripta Mater. 48 (2003) 099.
[10] M. Yamagay, P.I. Macfarlane, B. Keith Holliday, K. Henderson, Y. Inoue, J. Phys. Condens. Matter 9 (1997) 1575.
[11] M. Yamaga, J.P.R. Wells, M. Honda, T.P.J. Han, B. Henderson, J. Lumin. 108 (2004) 313.
[12] T. Ohtake, N. Sonoyama, T. Sakata, Chem. Phys. Lett. 318 (2000) 517.
[13] W. Ryba-Romanowski, S. Gołab, W.A. Pisarski, G. Dominiak-Dzik, M.N. Palatnikov, N.V. Sidorov, V.T. Kalinnikov, Appl. Phys. Lett. 70 (1997) 2505.
[14] T.P.J. Han, F. Jaque, L. Arizmendi, V. Bermudezb, A. Suchocki, J. Lumin. 108 (2004) 55.
[15] X. Long, G. Wang, T.P.J. Han, J. Cryst. Growth 249 (2003) 191.
[16] A. Al-Abdalla, Z. Barandiaran, L. Seijo, R. Lindh, J. Chem. Phys. 108 (1998) 2005.
[17] O.S. Wenger, R. Valiente, H.U. Gudel, J. Chem. Phys. 115 (2001) 3819.
[18] R.J.M. da Fonseca, A.D. Tavares Jr., P.S. Silva, T. Abritta, N.M. Khaidukov, Solid State Commun. 110 (1999) 519.
[19] M. Mortier, Q. Wang, J.Y. Buzare, M. Rousseau, B. Piriou, Phys. Rev. B 56 (1997) 3022.
[20] J.J. Kingsley, K. Suresh, K.C. Patil, J. Mater. Sci. 25 (1990) 1305.
[21] J.J. Kingsley, K.C. Patil, Bull. Mater. Sci. 13 (1990) 179.
[22] L.E. Shea, J. McKittrick, O.A. Lopez, J. Am. Ceram. Soc. 79 (12) (1996) 3257.
[23] S.H.M. Poort, W.P. Blockpoel, G. Blasse, Chem. Mater. 7 (1995) 1547.
[24] T. Matsuzawa, Y. Aoki, N. Takeuchi, Y. Murayama, J. Electrochem. Soc. 143 (1996) 2670.
[25] B.M. Mohamed, J.H. Sharp, J. Mater. Chem. 7 (1997) 1595.
[26] J.J. Kingsley, K.C. Patil, Mater. Lett. 6 (1988) 427.
[27] G. Fuxi, Optical and Spectroscopic Properties of Glass, Springer, Berlin, 1992, p. 136.
[28] A. Carrington, A. McLahlan, Introduction to Magnetic Resonance, Harper, New York, 1967.
[29] A. Abragam, B. Bleaney, Electron Paramagnetic Resonance of Transition Ions, Clarendon, Oxford, 1970.
[30] R. Knutson, H. Liu, W. Yen, T. Morgan, Phys. Rev. B 40 (1989) 4264.
[31] J.A. Weil, J.R. Bolton, J.E. Wertz, Electron Paramagnetic Resonance-Elementary Theory and Practical Applications, Wiley, New York, 1994, p. 498.
[32] N.W. Aschcroft, N.D. Mermin, Solid State Physics, Harcourt College Publishers, 2001, p. 656.
[33] S.B. Berger, J. Appl. Phys. 36 (19651048).
[34] D.L. Wood, G.F. Imbusch, R.M. Macfarlane, P. Kisliuk, D.M. Larkin, J. Chem. Phys. 48 (1968) 5255.
[35] R.A. Ford, O.F. Hill, Spectrochim. Acta 16 (1960) 1318.
[36] M. Yamaga, H. Takeuchi, T.P.J. Hahn, B. Henderson, J. Phys.: Condens. Matter 5 (1993) 8097.
[37] Y. Tanabe, S. Sugano, J. Phys. Soc. Japan 9 (753) (1954) 766.
[38] G. Lorenzi, G. Baldi, Francesco Di Benedetto, Valentina Faso, Luca A. Pardi, Maurizio Romanelli, J. Eur. Ceram. Soc. 26 (2006) 125.
[39] J.W. Orton, An Introduction to Transition Group Ions in Crystals, ILIFFE Book Ltd., London, 1968.
[40] X. Long, Z. Lin, Z. Hu, G. Wang, T.P.J. Han, J. Alloys Compd. 347 (2002) 52.